Imaging of reflective surfaces by near-field optics

Gang Bao[1] **and Junshan Lin**[2]

[1] *Department of Mathematics, Zhejiang University, Hangzhou, China;*
and Department of Mathematics, Michigan State University, East Lansing, MI 48824, USA.
[2] *Institute for Mathematics and its Applications, University of Minnesota,*
Minneapolis, MN 55455, USA
[*] *Corresponding author: Junshan Lin*

We consider an imaging problem which aims to identify the profile of a reflective surface by the scattered wave measured in the near field. Potential applications include nondestructive detection of micro devices, subwavelength imaging techniques in nano-optics. When the height of the imaging target is small, the connection between the localized evanescent wave modes of the measurement and the high spatial frequency components of the structure is characterized explicitly, which leads to a natural reconstruction method with super resolution images. A novel multiple frequency approach is also presented which captures both the main features as well as the fine details of the structure.

Near-field optics has been an active research field in the past few decades, motivated by applications in near-field microscopies for breaking the diffraction limit. There exist various configurations of near-field microscopies, including the near-field scanning optical microscopy (NSOM) [11, 14] and the scanning tunneling optical microscope (STOM) [12,16]. In general, high resolution in the near field is provided by taking into account of evanescent waves. In principle, arbitrary resolution can be achieved by near-field microscopies, provided that the bandwidth is infinite. However, this is at the expense of strong coupling between the source and the imaging object. Moreover, the images obtained from near-field microscopies are problematic by visualizing the object in an analogical way [5, 15]. To overcome the difficulty the inverse scattering theory has been applied to understand how the structure of the scattering object is encoded in the measured scattered field. Under the weak scattering or the Born approximation, recent results may be found in [6, 7] for the near-field scanning optical microscopy (NSOM) and the total internal reflection microscopy (TIRM) .

This letter is devoted to a nonliner imaging problem. We are concerned with imaging some reflective surface on a ground plane by the data measured in the near-field regime (Figure 1). We refer to [13] for a linearized model of the nonlinear problem under the Born approximation. In general, the inversion becomes much more challenging when the problems are nonlinear. Two imaging techniques are presented in this letter. One is based on the plane wave decomposition of the scattered wave and boundary integral equations, which yields super resolution when the height of the imaging target is small. The other relies on the multiple frequency data, where at fixed frequency a minimization problem is solved. In particular, the latter is capable of imaging profiles with multiple scales.

We focus on the two dimensional problem by assuming that the whole object is an infinite cylinder. The surface of the object is illuminated by a time-harmonic

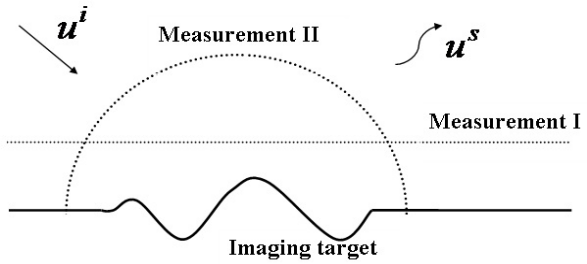

Fig. 1. Problem geometry.

electromagnetic wave $u^i = e^{ikd\cdot x}$ that propagates along the direction d, where k is the wavenumber. The total field u consists of three parts: the incident wave u^i, the reflected wave u^r by the ground plane, and the scattered field u^s. The total field u satisfies the Helmholtz equation for the TM polarized case:

$$\Delta u + k^2 u = 0 \quad \text{above the ground plane.} \tag{1}$$

By assuming that the surface is perfectly reflective, the total field vanishes on the boundary. In addition, at infinity the scattered field u^s satisfies the Sommerfeld radiation condition [10].

Let $x = (x_1, x_2)$, applying the layer potential theory [3, 10], the scattered field u^s can be expressed as the single layer potential

$$u^s(x) = \int_\Gamma G(x,y)\psi(y)ds_y \tag{2}$$

with a density function ψ. Here and henceforth, Γ represents the profile of the reflective surface, the Green's function is defined via

$$G(x,y) := \Phi(x,y) - \Phi(x_r,y). \tag{3}$$

$\Phi(x,y) = \frac{i}{4}H_0^{(1)}(k|x-y|)$ is the fundamental solution for the Helmholtz equation in $\mathbf{R}^2$ and x_r is the reflection of x by the x_1 axis.

The connection between the scattered wave modes and the profile is well understood with the following plane wave decomposition:

$$\Phi(x,y) = \frac{i}{4\pi}\int_{-\infty}^{\infty} \frac{1}{k_2(\kappa)} e^{i(x_1-y_1)\cdot\kappa} e^{ik_2(\kappa)|x_2-y_2|} d\kappa,$$

where $k_2(\kappa) = \sqrt{k^2 - |\kappa|^2}$ for $|\kappa| < k$ (propagating modes), and $k_2(\kappa) = i\sqrt{|\kappa|^2 - k^2}$ for $|\kappa| > k$ (evanescent modes). A similar plane wave decomposition for $G(x,y)$ implies that the scattered field u^s is a superposition of the propagating and evanescent wave modes. Such evanescent wave modes are localized to the surface, and are significant in the near-field regime. They carry the fine feature information of the object to be reconstructed.

Let the function f represent the profile of the reflective surface, which vanishes outside a bounded interval γ, i.e., the imaging target $\Gamma := \{x = (x_1, x_2) \mid x_1 \in \gamma,\ x_2 = f(x_1)\}$. First, consider the case when data is measured on the line $x_2 = d$ above the structure with a distance that is smaller than the wavelength λ (Measurement I Figure 1). Assume that the height of the object is small in the sense that $\left(\frac{f}{\lambda}\right)^2 \ll 1$, then the connection between the evanescent wave modes and the high frequency components of the imaging target are formulated explicitly as follows:

$$\hat{u}^s(\kappa, d) \approx e^{ik_2(\kappa)d}\widehat{(f\varphi)}(\kappa), \quad \kappa \in (-\infty, \infty), \qquad (4)$$

where $\widehat{\cdot}$ denotes the Fourier transform, and $\varphi = \psi\sqrt{1 + |f'|^2}$. Note that when the magnitude of the spatial frequency $|\kappa| > k$, the transfer function $e^{ik_2(\kappa)d}$ decreases exponentially with respect to the distance d. In the near-field regime, such exponentially decayed modes are still significant, thus the high spatial frequency components of f may be retrieved.

The first step of the reconstruction is to retrieve $f\varphi$ in the spatial frequency domain. This is a linear ill-posed problem. By the relation (4), we introduce the pseudo-inverse operator $\mathbf{I}_d$:

$$\mathbf{I}_d(\kappa) = \begin{cases} e^{-ik_2(\kappa)d} & |\kappa| \le k_c, \\ 0 & |\kappa| > k_c\,, \end{cases}$$

where, for a noise level σ, the cut-off frequency k_c is chosen such that $e^{ik_2(k_c)d} = e^{-\sqrt{k_c^2 - k^2}\,d} = \sigma$. Let

$$\hat{h}(\kappa) = \mathbf{I}_d(\kappa)\hat{u}^s(\kappa, d).$$

Then it is clear that h, the inverse Fourier transform of $\hat{h}(k)$, is a bandlimited approximation of $f\varphi$ with bandwidth $k_c = \left(k^2 + \left(\frac{\log\frac{1}{\sigma}}{d}\right)^2\right)^{1/2}$. It is obvious that at the fixed noise level, the bandwidth of the recovered spatial frequency in the near field is much larger than in the far field. For example, for a 5% noise level, $k_c \approx 2.6k$ when the measurement distance $d = 0.2\lambda$. i.e., the near-field cut-off frequency is more than twice of that of the far-field, which equals k.

The second step of the reconstruction is to separate f from h by matching the Dirichlet data on the boundary. This requires solving a nonlinear well-posed problem:

$$\min \|K_f\varphi + g_f\|_{L^2(\gamma)} \quad \text{where} \qquad (5)$$
$$\varphi \ \text{ is a continuous function that satisfies } f\varphi = h.$$

$g_f(x_1)$ is the sum the incident field $u^i(x)$ and the reflected field $u^r(x)$ with $x = (x_1, f(x_1))$. The integral operator K_f is given by

$$(K_f\varphi)(x_1) := \int_{\tilde{\gamma}} \tilde{G}(x_1 - y_1; f(x_1), f(y_1))\varphi(y_1)dy_1,$$

where the kernel $\tilde{G}(x_1 - y_1; f(x_1), f(y_1))$ is the Green's function defined by (3) with $x = (x_1, f(x_1))$ and $y = (y_1, f(y_1))$. From the single layer potential (2), we see that $K_f\varphi$ is the scattered field on the reflective surface. Thus by minimizing the cost functional we enforce the Dirichlet boundary condition. The minimization problem (5) can be solved efficiently by the Newton's method.

We present an example where the imaging target consists of two bumps separated with a distance of $\frac{\lambda}{10}$, and the measurement distance $d = \frac{\lambda}{5}$. The reconstruction with a 5% noise level in measurements is shown in Figure 2, which clearly demonstrates the super resolution image obtained by the current imaging method.

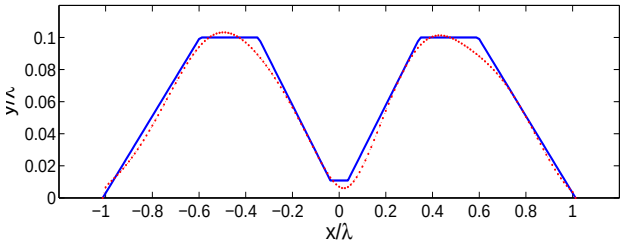

Fig. 2. Near-field image (dotted line) and the real profile (solid line).

We next consider very general cases without any restriction on the height of reflective surface. Multiple frequency measurements are taken. More specifically, in our model the scattered field u^s is measured on the half circle ∂B_R^+ with radius R for different frequencies $\omega_1, \omega_2, \cdots, \omega_M$ (Measurement II in Figure 1).

Introduce the forward mapping $\mathcal{S}$ that maps Γ to the total field u on the half circle ∂B_R^+. A continuation approach is employed to image the reflective surface. By starting from the smallest frequency ω_1, the method marches from low to high frequencies, where at fixed frequency ω, the nonlinear imaging problem is recast as an optimization problem:

$$\min \tfrac{1}{2}\|\mathcal{S}(\Gamma) - u_{meas}\|^2_{L^2(\partial B_R^+)} =: \min \mathcal{J}(\Gamma).$$

$u_{meas} = u^s_{meas} + u^i + u^r$ is the measurement of the total field. To be more specific, a smooth descent direction V for the cost functional $\mathcal{J}(\Gamma)$ is defined, and the profile is updated with V.

We choose V such that

$$-\int_\Gamma (V \cdot n) \cdot Real \left\{ \frac{\partial u}{\partial n} \frac{\partial \bar{u}_{adj}}{\partial n} \right\} ds < 0,$$

wherein u and u_{adj} are the solutions of the forward problem (1) and the adjoint problem respectively, and n is the unit normal on Γ directed into the infinite domain above the ground plane. We refer to [4] for a detailed proof that such V serves a descent direction. The adjoint problem is defined as follows:

$$\begin{cases} \Delta u_{adj} + k^2 u_{adj} = 0 & \text{above the ground plane,} \\ u_{adj} = 0 & \text{on } \Gamma, \\ \frac{\partial u^{adj}}{\partial n} = \mathcal{T}^*(u_{adj}) + u - u_{meas} & \text{on } \partial B_R^+. \end{cases}$$

where $\mathcal{T}^*$ is the adjoint operator of the Dirichlet-to-Neumann operator $\mathcal{T}(u \to \dfrac{\partial u}{\partial n})$.

Such continuation approach from ω_1 to ω_M overcomes the difficulty of reaching some local minima for the optimization problem at fixed frequency. Moreover, by marching to a higher frequency, it is expected more details of the profile can be captured, as shown in the example below. We also refer to [1,2,9] for studies of such continuation approaches been applied to solve related inverse scattering problems.

In general, the lowest frequency ω_1 is small to guarantee that the main features of the imaging target are captured. We insist that the wavelength λ_1 corresponding to the lowest frequency is at least comparable to the support of Γ. The forward and the adjoint problems can be solved efficiently by the boundary integral equation method. We refer to [4] for more details and other practical considerations of the method.

Let us consider a profile with two scales: the order of the large scale feature is 1.0 while the order of the small scale feature is 0.1. Figure 3 is the reconstruction images for various wavenumbers with a 5% noise level. The method leads to a convergent reconstruction, where at $k = 5$ the main features of the profile are well recovered and the small scale features (two bumps) are captured at $k = 20$. The corners of two bumps are furthered recovered when k increases.

The research of GB was supported in part by the NSF grants DMS-0908325, DMS-0968360, DMS-1211292, the ONR grant N00014-12-1-0319, a Key Project of the Major Research Plan of NSFC (No. 91130004), and a special research grant from Zhejiang University.

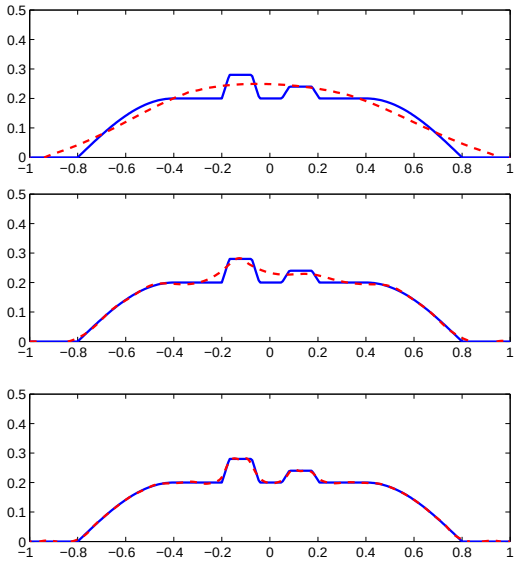

Fig. 3. Evolution of the reconstruction at $k = 5, 20, 40$. The dash line is the reconstruction, and the solid line is the real image.

References

1. G. Bao and P. Li, Opt. Lett., **32**, 1465 (2007).
2. G. Bao and P. Li, Inverse Problems, **20**, L1 (2004).
3. G. Bao and J. Lin, Inverse Probl. Imag., to appear.
4. G. Bao and J. Lin, SIAM J. Appl. Math. **71**, 1733 (2011).
5. R. Carminati and J. Greffet, J. Opt. Soc. Am. A, **12**, 2716 (1995).
6. P. Carney and J. Schotland, Appl. Phys. Lett. **77**, 2798 (2000).
7. P. Carney and J. Schotland, Opt. Lett. **26**, 1072 (2001).
8. P Chaumet, K. Belkebir, and A. Sentenac, Phy. Rev. A, **76**, 013814 (2007).
9. Y. Chen, Inverse Problems, **13**, 1 (1997).
10. D. Colton and R. Kress, *Integral Equation Methods in Scattering Theory*, Pure and Applied Mathematics (1983).
11. D. Courjon and C. Bainier, Rep. Prog. Phys., **57**, 989 (1994).
12. D. Courjon, K. Sarayeddine, and M. Spajer, Opt. Commun., **71**, 23-28 (1989).
13. G. Derveaux, G. Papanicolaou and C. Tsogka, Inverse Problems **22**, 1437, (2006).
14. R. Dunn, Chem. Rev., **99**, 2891 (1999).
15. D. Labeke and D. Barchiesi, J. Opt. Soc. Am. A , **9**, 732 (1992).
16. R. C. Reddick, R. J Warmack, D. W. Chilcott, S. L. Sharp , and T. L. Ferrel, Rev. Sci. Instrum., **61**, 3669 (1990).

References

1. G. Bao and P. Li, *Numerical solution of inverse scattering for near-field optics*, Opt. Lett., **32** (2007), 1465-1467.
2. G. Bao and P. Li, *Inverse medium scattering for three-dimensional time harmonic Maxwell equations*, Inverse Problems, **20** (2004), L1-L7.
3. G. Bao and J. Lin, *Near-field imaging of the surface displacement on an infinite ground plane*, Inverse Probl. Imag., to appear.
4. G. Bao and J. Lin, *Imaging of local surface displacement on an infinite ground plane: the multiple frequency case*, SIAM J. Appl. Math. **71** (2011), 1733-1752 .
5. R. Carminati and J. Greffet, *Influence of dielectric contrast and topography on the near field scattered by an inhomogeneous surface*, J. Opt. Soc. Am. A, **12** (1995), 2716-2725.
6. P. Carney and J. Schotland, *Inverse scattering for near-field microscopy*, Appl. Phys. Lett. **77** (2000), 2798-800.
7. P. Carney and J. Schotland, *Three-dimensional total internal reflection microscopy*, Opt. Lett. **26** (2001), 1072-1074.
8. P Chaumet, K. Belkebir, and A. Sentenac, *Numerical study of grating-assisted optical diffraction tomography*, Phy. Rev. A, **76** (2007), 013814.
9. Y. Chen, *Inverse scattering via Heisenberg's uncertainty principle*, Inverse Problems, **13** (1997), 1-13.
10. D. Colton and R. Kress, *Integral Equation Methods in Scattering Theory*, Pure and Applied Mathematics, Wiley, New York (1983).
11. D. Courjon and C. Bainier, *Near field microscopy and near field optics*, Rep. Prog. Phys. **57** (1994), 989-1028.
12. D. Courjon, K. Sarayeddine, and M. Spajer, *Scanning tunneling optical microsocpy*, Opt. Commun. **71** (1989), 23-28.
13. G. Derveaux, G. Papanicolaou and C. Tsogka, *Resolution and denoising in near-field imaging*, Inverse Problems **22** (2006), 1437-1456.
14. R. Dunn, *Near-Field Scanning Optical Microscopy*, Chem. Rev. **99** (1999), 2891-2927.
15. D. Labeke and D. Barchiesi, *Scanning-tunneling optical microscopy: a theoretical macroscopic approach*, J. Opt. Soc. Am. A **9** (1992), 732-739.
16. R. C. Reddick, R. J Warmack, D. W. Chilcott, S. L. Sharp , and T. L. Ferrel, *Photon scanning tunneling microscopy*, Rev. Sci. Instrum. **61** (1990) 3669-3677.